Equation of Motion for a Grain Boundary

Luchan Zhang, Jian Han, Yang Xiang, and David J. Srolovitz

Phys. Rev. Lett. **119**, 246101 — Published 12 December 2017

DOI: 10.1103/PhysRevLett.119.246101

The Equation of Motion for a Grain Boundary

Luchan Zhang,[1, 2] Jian Han,[1] Yang Xiang,[2, *] and David J. Srolovitz[1, 3, 4, †]
[1]*Department of Materials Science and Engineering, University of Pennsylvania, Philadelphia, PA 19004 USA*
[2]*Department of Mathematics, The Hong Kong University of Science and Technology, Clear Water Bay, Kowloon, Hong Kong*
[3]*Department of Mechanical Engineering and Applied Mechanics, University of Pennsylvania, Philadelphia, PA 19004 USA*
[4]*Institute for Advanced Study, The Hong Kong University of Science and Technology, Clear Water Bay, Kowloon, Hong Kong*

Grain boundary (GB) migration controls many forms of microstructural evolution in polycrystalline materials. Recent theory, simulations and experiments demonstrate that GB migration is controlled by the motion of discrete line defects/disconnections. We present a continuum equation of motion for grain boundary derived from the underlying discrete disconnection mechanism. We also present an equation of motion for the junctions where multiple grain boundaries meet – as is always the case in a polycrystal. The resulting equation of motion naturally exhibits junction drag – a widely observed phenomena in junction dynamics in solids and liquids.

A polycrystalline material may be thought of as an ensemble of crystalline grains or, on the mesoscale as a network of grain boundaries (GBs) – GBs are the interfaces between these differently oriented crystalline grains. Because this GB network has a large impact on a wide range of material properties (e.g., strength, toughness, corrosion resistance, electrical conductivity [1]), its evolution is important for engineering materials. The temporal evolution of the GB network occurs through GB migration. Since GBs are interfaces between crystals, the microscopic mechanisms by which they move are intrinsically different from other classes of interfaces (e.g., solid/liquid interfaces, surfactant interfaces in micelles, biological cell membranes). The microscopic mechanism of GB migration is associated with the motion of topological line defects (disconnections) in the interface that result from the symmetry of the bounding crystals. This crystallography dependence has a profound effect on GB migration; e.g., GB migration may be driven by stresses, in addition to such effects as capillarity that describe the motion of other interfaces. While the motion of other classes of interfaces (in non-crystalline matters) has been widely studied on the mesoscale, a mesoscale description of GB motion (based on its underlying microscopic mechanism) is missing. In this Letter, we propose a continuum equation of motion for GBs based on the underlying microscopic mechanisms and integrates the effects of a diverse range of thermodynamic driving forces.

Experimental evidence has been accumulating that GBs move in response to shear stresses [2, 3] (in addition to other driving forces [4–6]); we refer to this phenomenon generically as shear-coupled GB migration. More recent theoretical, simulation [7–11] and experimental work [3] has shown that the GB velocity is proportional to shear stress and switches sign upon reversal of the sense of the shear. There is also a growing body of evidence that shear-coupled GB migration occurs through the motion of line defects [12, 13] which may generally be referred to as disconnections [14–16]. Disconnections are characterized by both step (step height H) and dislocation character (Burgers vector $\mathbf{b}$) [16]. The possible $(\mathbf{b}, H)$ pairs for a disconnection are determined solely by the GB crystallography; more specifically for a coincidence-site-lattice GB, $\mathbf{b}$s are translation vectors of the bicrystal lattice [17] and the set of possible Hs are crystallographically determined for each $\mathbf{b}$ [14]. While stresses couple to the Burgers vector to move the disconnections, disconnections may also move in response to driving forces that couple to the step height (akin to step flow on a growing surface).

Figure 1 shows a GB composed of flat sections and disconnections. The motion of disconnections in the same direction translates the GB while motion of disconnections towards (and annihilating with) each other changes the GB curvature. Hence, both GB migration and change in GB shape can be characterized by disconnection motion. We assume that disconnection motion is overdamped such that the velocity is $v_\mathrm{d} = M_\mathrm{d} f_\mathrm{d}$, where f_d is the force on the disconnection and M_d is its mobility (the constant relating driving force to velocity which may, in general, be affected by local bonding, GB structure, solute segregation, point defects, etc.).

In this model we consider GB migration via the motion of a single disconnection type that glides along a GB (its Burgers vector is in the GB plane;

see Fig. 1). Although other disconnections may exist (with components of $\mathbf{b}$ perpendicular to the GB plane), the motion of these tend to be slow and require diffusion (relatively unimportant for GB migration). Although, at high temperature disconnections of multiple types may be activated, MD simulations [7] shows that shear coupling tends to be dominated by a single disconnection type except at very high temperature (close to the melting point in many cases) for most GBs.

The driving force on a disconnection has two terms $f_\mathrm{d} = f_\tau + f_\mathrm{B}$. The first term is associated with the coupling of the disconnection Burgers vector to the stress $\boldsymbol{\sigma}$ (i.e., Peach-Koehler force): $f_\tau = (\boldsymbol{\sigma} \cdot \mathbf{b} \times \boldsymbol{\xi}) \cdot \hat{\mathbf{g}}$, where $\boldsymbol{\xi}$ is the disconnection line direction and $\hat{\mathbf{g}}$ is the glide direction of the disconnection [18]. The second term couples the motion of the disconnection step to the energy reduction in the system. This term may be associated with the energy jump across the GB Ψ; e.g., associated with dislocation density (i.e., the driving force for primary recystallization), elastic energy (from elastic anisotropy), or artificial energy density differences (as used in many atomistic simulations of GB migration [19]).

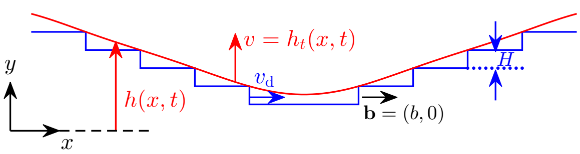

FIG. 1. A GB with disconnections (blue curve) and its continuum representation $y = h(x,t)$ (red curve). The GB velocity v (in the y-direction) results from disconnection glide characterized by $(\mathbf{b}, H)$ and $(-\mathbf{b}, -H)$ in the x-direction.

On the continuum level, a GB may be modeled as a smooth curve (surface), as shown in Fig. 1. We assume that the GB "terraces" are parallel to the x-direction, the GB shape is $y = h(x,t)$, and the disconnection density is small ($|h_x| \ll 1$; h_x is the signed disconnection density). The driving force for disconnection motion associated with stress is $f_\tau = (\sigma_\mathrm{i} + \tau) b h_x / |h_x|$, where σ_i is the stress from all the disconnections in the system and τ is the applied stress. If all the disconnections lie on a single GB, the stress due to the elastic interaction between disconnections is [18]

$$\sigma_\mathrm{i}(x,t) = K \int_{-\infty}^{\infty} \frac{\beta h_x(x_1,t)}{x - x_1} dx_1, \quad (1)$$

where $K = \mu/[2\pi(1-\nu)]$, μ is the shear modulus, ν is the Poisson ratio, and $\beta \equiv b/H$ is the shear-coupling factor [7, 20]. The stress field $\boldsymbol{\sigma}_\mathrm{i}$ due to the long-range elastic interaction of disconnections that locate on multiple GBs in a two-dimensional microstructure can also be calculated from the stress field of dislocations [18] (see Supplemental Material, SM).

The bicrystal driving force f_B is determined from the variation of the energy of the bicrystal (with GB length L) $E = \int_0^L (\Psi h + \gamma \sqrt{1 + h_x^2}) dx$ with respect to the displacement of the disconnection, u. Using $\delta E/\delta u = (H/L) \delta E/\delta h$, we have

$$f_\mathrm{B} = \left(-\frac{\delta E}{\delta u}\right)\left(-\frac{h_x}{|h_x|}\right) = (\Psi - \gamma h_{xx}) H \frac{h_x}{|h_x|}, \quad (2)$$

where $|h_x| \ll 1$. This expression explicitly accounts for the GB curvature (Gibbs-Thomson effect) with GB energy γ and the energy jump across the GB Ψ.

We relate the evolution of the GB profile $h(x,t)$ to the disconnection velocity as $h_t + v_\mathrm{d} h_x = 0$. This implies that, if a GB is initially flat ($h_x = 0$), it will always remain flat. Hence, neither an applied stress τ nor an energy jump Ψ will be able to move an initially flat GB, despite simulation and experimental observations to the contrary [3, 7]. This would be true at $T = 0$ for a faceted GB; however, at finite T there is a thermal equilibrium disconnection concentration at any finite driving force. Since disconnections form in pairs (or as loops in three dimensions), we can write the equilibrium disconnection concentration (in analogy to thermal equilibrium of kinks on a dislocation [18]) as $c_\mathrm{e}(T) = (1/a) e^{-F_\mathrm{d}/(k_\mathrm{B} T)}$, where F_d is half the disconnection pair formation energy, a is an atomic spacing and k_B is the Boltzmann constant. We note that it is this thermal density of disconnections that gives rise to GB roughening [21].

Lateral motion of these thermal disconnections under finite driving force leads to the motion of a nominally flat GB. Inclusion of this effect in the equation of GB motion yields $h_t + v_\mathrm{d} h_x = 2 c_\mathrm{e} H v_\mathrm{d} (h_x/|h_x|)$. Collecting all of these terms leads to the following continuum equation of GB motion:

$$h_t = -M_\mathrm{d}[(\sigma_\mathrm{i} + \tau) b + \Psi H - \gamma h_{xx} H](|h_x| + B), \quad (3)$$

where $B = 2 H c_\mathrm{e}(T)$. The velocity of each GB segment has both local terms (second and third terms in the square brackets) and a non-local term (associated with the spatial distribution of disconnections throughout the microstructure as embodied in σ_i). See SM for the detailed derivation.

We now apply Eq. (3) to numerically solve two GB dynamics problems using a finite-difference approach. The materials constants are chosen to represent a $\Sigma 5$ [100] (310) 36.87° symmetric tilt GB

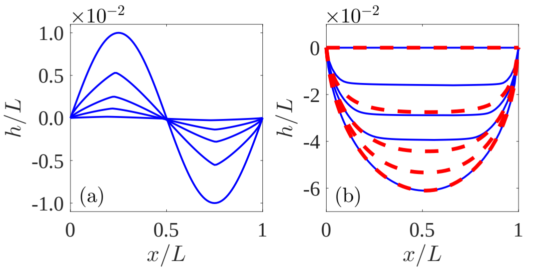

FIG. 2. (a) Numerical solution for the evolution of a GB from an initially sinusoidal profile for no externally applied force $\tau = 0$ and $\Psi = 0$ and $B = 0$. The GB profile is shown for $t = 0$, $2t_0$, $6t_0$, $15t_0$, and ∞, where $t_0 = L/(M_{\mathrm{d}}\gamma)$. (b) The evolution of a GB pinned at two junctions for $\tau = 5 \times 10^{-2}\mu$ at $t = 0$, $5t_0$, $10t_0$, $15t_0$, and ∞ for $B = 0.01$ (blue) and $t = 0$, t_0, $2t_0$, $3t_0$, and ∞ for $B = 0.1$ (red).

in aluminum (see SM for details of the numerical method and choice of parameters). The first application is to the capillarity-driven flattening of a sinusoidally perturbed GB profile; there is no applied stress ($\tau = 0$) or energy jump across the GB ($\Psi = 0$).

Figure 2a shows that an initially perturbed GB profile evolves to a flat profile even at $T = 0$ ($B = 0$). Although flattening is expected based on motion by mean curvature and the capillary term is indeed included in Eq. (3), the dominant driving force in our simulations is the long-range elastic interaction between disconnections ($\sigma_{\mathrm{i}} \neq 0$). We see that, although the GB starts smooth and ends flat, sharp corners form at the extrema of the profile and the corresponding jump in slope tends to zero as the GB becomes flat. This results from the $|h_x|$ term that gives rise to the discontinuity in the slope at the extrema of the GB profile. This is a dynamics, rather than energetics, effect.

Our next example is an initially flat GB pinned between two points, such as may occur where a GB is delimited by two stationary GB triple junctions (TJs) – of course, in a real polycrystal, TJs are not fixed (we return to mobile TJs below). This case is shown in Fig. 2b, where the GB migration is driven by the stress $\tau = 5 \times 10^{-2}\mu$ ($\Psi = 0$). Since a flat GB will not move without disconnections, we set $B = 0.01$ (blue) and 0.1 (red). Larger values of B correspond to higher temperature. Figure 2b shows that the applied stress/shear coupling causes the GB to bow out between the pinning points from the initially flat profile to a time-independent (equilibrium) shape at late time. Such disconnection pair nucleation induced GB curvature has been experimentally observed [22]. While the detailed shape (and rate of evolution) of the evolving

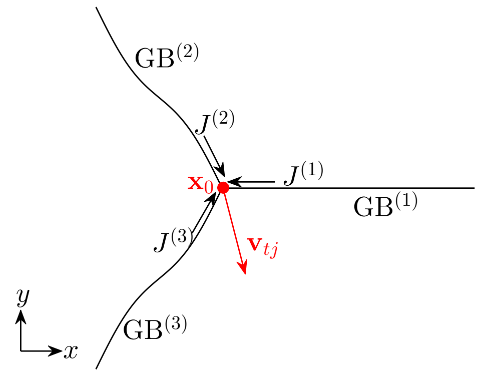

FIG. 3. Illustration of TJ motion (red arrow) through disconnection fluxes from three GBs.

GB is different for different values of B (or T), the late-time, stationary shape is independent of B (the equilibrium profile is determined by a balance between the driving forces due to the applied stress, the elastic interactions between disconnections, and capillarity). Also note that, unlike in the evolution without thermal disconnection ($B = 0$) in Fig. 2a, here no corners form in the evolving profile. This is a consequence of the inclusion of a non-zero equilibrium disconnection density B in Fig. 2b, which regularizes the discontinuity associated with $|h_x|$ in Eq. (3). Not surprisingly, larger equilibrium disconnection densities (larger B) lead to faster evolution.

While the previous TJ-pinned GB evolution example (Fig. 2b) provides insight into how a finite-size GB profile may evolve, it is not a good representation of a GB in a polycrystal. If the TJs do not move, the average grain size would not evolve; there would be no grain growth. At the same time, disconnections cannot move across TJs because the GBs meeting there will, in general, have distinct $(\mathbf{b}, H)$ sets.

The disconnection flux into a TJ will translate the TJ; disconnections from different GBs may react (and partially annihilate) at the TJ – see Fig. 3. Here we present a model for TJ motion based on the conservation of disconnection step height and Burgers vector at a TJ. The displacement of TJ is a consequence of disconnection steps flowing into the TJ. TJ motion influences the evolution of (motion of disconnections on) the three GBs via continuity conditions and Burgers vector accumulation at the TJ creates a back stress on the disconnections on the GBs. This means that TJ motion appropriately accounts for both the step and Burgers vector fluxes at the TJ and feeds back into the motion of the three GBs meeting there. See SM for details.

Following this approach, the TJ velocity $\mathbf{v}_{\mathrm{tj}}$ at

$\mathbf{x}_0$ is proportional to the total inward disconnection flux $J(\mathbf{x}_0)$ along each of the three GBs meeting at the TJ:

$$\mathbf{v}_{\rm tj} = -\sum_{i=1}^{3} H^{(i)} J^{(i)}(\mathbf{x}_0)\mathbf{n}^{(i)}, \quad (4)$$

where $\mathbf{n}^{(i)}$ is the normal to the reference (flat) GB$^{(i)}$, $J^{(i)}(\mathbf{x}_0) = (\rho^{(i)}(\mathbf{x}_0) + B/2)v_{\rm d}^{(i)}(\mathbf{x}_0)$ for disconnections moving toward the TJ (and $J^{(i)}(\mathbf{x}_0) = 0$ otherwise), $v_{\rm d}^{(i)}$ is the disconnection velocity along GB$^{(i)}$, and $\rho^{(i)}$ is the disconnection density at the TJ. $\rho^{(i)} = (\partial h^{(i)}/\partial s^{(i)})/H^{(i)}$ where $h^{(i)}$ is the GB profile measured in the $\mathbf{n}^{(i)}$ direction and $s^{(i)}$ is the arclength of GB$^{(i)}$ such that $(\mathbf{s}^{(i)}, \mathbf{n}^{(i)})$ forms a right-hand coordinate system. We note that the TJ may have an associated Burgers vector arising from the divergence of the Burgers vector flux there – the elastic field of this TJ Burgers vector interacts with the disconnections on the GBs (see SM).

Disconnection reactions at TJs require atomic rearrangement on the scale of GB width or disconnection core size and cannot be described solely on the basis of continuum descriptions. In the case where disconnection motion along the GBs is fast compared with the kinetics of disconnection reactions at the TJ, TJ motion is controlled by disconnection reactions at the TJs. In this case, the effective disconnection velocity at the TJ $v_{\rm d}^{(i)}(\mathbf{x}_0)$ should be replaced by a constant that relates to disconnection reaction rate constants at the TJ; i.e., $v_{\rm d}^{(i)}(\mathbf{x}_0) \to A^{(i)}$. In the $A^{(i)} \to 0$ limit, the TJ will not move, while in the $A^{(i)} \to \infty$ limit, the disconnections near the TJ move infinitely fast and the disconnection density at the TJ remains zero.

As an example of coupled GB and TJ migration, we consider a schematic, simplified model "microstructure" depicted in the inset of Fig. 4a; the system is periodic along the x-direction, is of infinite extent along y, and all GBs have identical properties. This is a very special case where in steady state, the flux of Burgers vectors into the TJ exactly cancel. A discussion of Burgers vector reaction at the TJ is discussed for more general cases in SM. In the absence of an external driving force on the GBs, the system equilibrates such that all GBs are flat and meet at the equilibrium angle $\theta_0 = 2\pi/3$. We drive the microstructure evolution by a uniaxial tensile stress, σ_{yy}, that produces equal and opposite shear on the GBs of opposite slopes and no shear on the vertical GBs. Because of the symmetry of the problem, the vertical GBs remain vertical and the TJs move only in the $\pm y$-direction. For this special case, the TJ/GB microstructure translates vertically at a steady-state velocity obtained by solving the continuum GB/TJ evolution Eqs. (3) and (4) as a function of the kinetic parameter ($0 \le A \le \infty$) via a finite-difference method (see SM). Figure 4a shows this steady-state microstructure and Fig. 4b shows the steady-state velocity of the GBs/TJs, as well as the steady-state TJ angles, $\theta_\wedge$ and $\theta_\vee$ (see Fig. 4a) as a function of A.

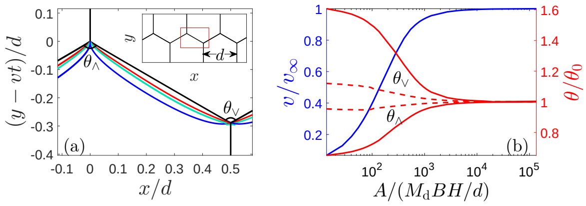

FIG. 4. (a) Equilibriu GB profiles for $A/(M_{\rm d}BH/d) =$ 0 (blue), 67.6 (green), 135.2 (red), and ∞ (black), at an applied shear stress $\tau = 5\times10^{-2}\mu$. (b) The steady-state GB velocity (blue line) and angles, $\theta_\wedge$ and $\theta_\vee$, as functions of A. The red solid (dashed) lines are the angles at equilibrium states for $\tau = 5\times10^{-2}\mu$ ($10^{-2}\mu$).

In the disconnection migration-controlled (large A) regime, the applied tensile stress drives the GB/TJ migration at a velocity $v_\infty = M_{\rm d}B\tau b$ such that the GBs remain flat and the TJ angles are at the equilibrium value, $\theta_\wedge = \theta_\vee = \theta_0$ (see Fig. 4). The fact that the translating GB shapes and TJ angles are identical to those in equilibrium (zero driving force) may be traced to the equilibrium disconnection density all along the GB (non-zero B in Eq. (3)) and the lack of a reaction barrier at the TJ. Note, however, these results (straight GBs and equilibrium angles) are special since the Burgers vectors from the disconnection cancel (in the x-direction) here, while in general they will not creating a back stress that will repel the disconnections from the TJ.

In the disconnection reaction-controlled (small A) regime, stress-driven GB migration leads to translation velocities $v < v_\infty$ and curved GBs. In the $A \to 0$ limit, the GB profile goes to a steady state (i.e., $v \to 0$), the GBs are strongly bowed and the TJ angles deviate from the equilibrium angles by up to 60% (for $\tau/\mu = 0.05$). As A increases (smaller reaction barriers at the TJs), the GBs and TJs move faster, become increasingly flat, and the TJ angles approach their equilibrium value θ_0. Figure 4b also shows that the magnitude of the deviation of the TJ angles from θ_0 increases with increasing applied stress (*cf.* the red lines in Fig. 4b). The deviation of the TJ angles from θ_0

with increasing velocity is consistent with observations in capillarity-driven GB migration [23, 24] and contact lines in fluid/solid systems [25].

The continuum equations of motion for GBs and TJs presented are based on a disconnection description of GB dynamics. A feature of the disconnection description is the existence of the coupling factor $\beta = b/H$ which relates to the underlying GB bicrystallography. While the bicrystallography admits infinitely many $(\mathbf{b}, H)$ sets for each GB [26], at low temperature the $(\mathbf{b}, H)$ set (and β) observed in experiment/atomistic simulation correspond to the lowest formation energy. As temperature increases, higher-energy $(\mathbf{b}, H)$ sets may be activated, changing the observed value of β (average over all the activated $(\mathbf{b}, H)$ sets). Also, the value of β observed may depend on the nature of the driving forces, since some couple to $\mathbf{b}$ and others to H. β may be determined based upon bicrystallography and a small number of atomistic simulations. Nonetheless, the equations of motion presented remain valid given the appropriate value of β.

ACKNOWLEDGEMENT

The authors gratefully acknowledge useful discussion with Spencer Thomas and Vaclav Vitek. The work of J.H. and D.S. was supported, in part, by the Center for the Computational Design of Functional Layered Materials, an Energy Frontier Research Center funded by the U.S. Department of Energy (DOE), Office of Science, Basic Energy Sciences (BES) under Award No. DE-SC0012575. L.C.Z. and Y.X. were partially supported by the Hong Kong Research Grants Council General Research Fund 606313.

REFERENCES

* maxiang@ust.hk

† srol@seas.upenn.edu

[1] A. P. Sutton and R. W. Balluffi, *Interfaces in Crystalline Materials* (Oxford University Press, 1995).
[2] C. H. Li, E. H. Edwards, J. Washburn, and E. R. Parker, Acta Metall. **1**, 223 (1953).
[3] M. Winning, G. Gottstein, and L. Shvindlerman, Acta Mater. **49**, 211 (2001).
[4] M. Seita, R. Schäublin, M. Döbeli, and R. Spolenak, Acta Mater. **61**, 6171 (2013).
[5] W. W. Mullins, Acta Metall. **4**, 421 (1956).
[6] C. V. Thompson, Ann. Rev. Mater. Sci. **20**, 245 (1990).
[7] J. W. Cahn, Y. Mishin, and A. Suzuki, Acta Mater. **54**, 4953 (2006).
[8] A. Rajabzadeh, F. Mompiou, M. Legros, and N. Combe, Phys. Rev. Lett. **110**, 265507 (2013).
[9] L.-L. Niu, Y. Zhang, X. Shu, F. Gao, S. Jin, H.-B. Zhou, and G.-H. Lu, Sci. Rep. **6**, 23602 (2016).
[10] X. H. Zhu and Y. Xiang, J. Mech. Phys. Solids **69**, 175 (2014).
[11] L. C. Zhang and Y. Xiang, arXiv (2017).
[12] K. L. Merkle, L. J. Thompson, and F. Phillipp, Interface Sci. **12**, 277 (2004).
[13] A. Rajabzadeh, M. Legros, N. Combe, F. Mompiou, and D. A. Molodov, Phil. Mag. **93**, 1299 (2013).
[14] A. H. King and D. A. Smith, Acta Cryst. **A36**, 335 (1980).
[15] J. P. Hirth, R. C. Pond, and J. Lothe, Acta Mater. **55**, 5428 (2007).
[16] J. P. Hirth and R. C. Pond, Acta Mater. **44**, 4749 (1996).
[17] R. W. Balluffi, A. Brokman, and A. H. King, Acta Metall. **30**, 1453 (1982).
[18] J. P. Hirth and J. Lothe, *Theory of Dislocations, 2nd ed.* (John Wiley, New York, 1982).
[19] K. G. F. Janssens, D. Olmsted, E. A. Holm, S. M. Foiles, S. J. Plimpton, and P. M. Derlet, Nat. Mater. **5**, 124 (2006).
[20] M. F. Ashby, Surf. Sci. **31**, 498 (1972).
[21] A. Karma, Z. T. Trautt, and Y. Mishin, Phys. Rev. Lett. **109**, 095501 (2012).
[22] R. C. Pond and S. Celotto, Int. Mater. Rev. **48**, 225 (2003).
[23] U. Czubayko, V. G. Sursaeva, G. Gottstein, and L. S. Shvindlerman, Acta Mater. **46**, 5863 (1998).
[24] D. Mattissen, D. A. Molodov, L. S. Shvindlerman, and G. Gottstein, Acta Mater. **53**, 2049 (2005).
[25] Y. Yuan and T. R. Lee, in *Surface science techniques* (Springer, 2013) pp. 3–34.
[26] F. Mompiou, M. Legros, and D. Caillard, Acta Mater. **58**, 3676 (2010).